PTEP

Prog. Theor. Exp. Phys. **2019**, 053B02 (12 pages)
DOI: 10.1093/ptep/ptz038

Probing CP-violating Higgs sectors via the precision measurement of coupling constants

Mayumi Aoki[1], Katsuya Hashino[2,3,*], Daiki Kaneko[1], Shinya Kanemura[3], and Mitsunori Kubota[3]

[1]*Institute for Theoretical Physics, Kanazawa University, Kanazawa 920-1192, Japan*
[2]*Department of Physics, University of Toyama, 3190 Gofuku, Toyama 930-8555, Japan*
[3]*Department of Physics, Osaka University, Toyonaka, Osaka 560-0043, Japan*
*E-mail: hashino@het.phys.sci.osakau.ac.jp

Received November 26, 2018; Revised March 5, 2019; Accepted March 19, 2019; Published May 17, 2019

We study how the effects of the CP violation can be observed indirectly by precision measurements of Higgs boson couplings at a future Higgs factory such as the International Linear Collider. We consider two Higgs doublet models with softly broken discrete symmetry. We find that by measuring the Higgs boson couplings very precisely we are able to distinguish the CP-violating two Higgs doublet model with a certain type of Yukawa interaction from the CP-conserving one.

Subject Index B40, B52, B53

1. Introduction

With the discovery of the Higgs boson (h), the standard model (SM) has been established as the low-energy effective theory below the electroweak scale [1,2]. In spite of such success of the SM, we do not think that the SM is a fundamental theory because there are several phenomena that cannot be explained in the SM, such as the baryon asymmetry of the universe (BAU), dark matter, neutrino mass, cosmic inflation etc. Therefore, an extension of the SM must be considered to describe these phenomena. This would be done at least partially by introducing an extended Higgs sector as seen in a promising scenario to explain BAU, the electroweak baryogenesis [3] where both additional CP-violating phases and strongly first-order electroweak phase transitions (EWPT) can occur in an extended Higgs sector.

Methods for exploring CP-violating effects in extended Higgs sectors have been studied by the electric dipole moment (EDM), angular distribution of $h \to \tau^-\tau^+$ [4–13], and the properties of new particles via collisions between protons, photons, or electrons and positrons [14–27]. Meanwhile, we can test the strongly first-order EWPT by measuring the SM-like Higgs coupling constants, especially the hhh coupling, which is enhanced by several tens of % from the SM prediction [28–38]. The effects of the strongly first-order EWPT can also be tested by detecting the characteristic spectrum of the gravitational waves that originate from the collision of the bubbles of the first-order EWPT [37–64].

In this paper, we examine how to indirectly detect the CP-violating effects by precision measurements of the SM-like Higgs boson in two Higgs doublet models (2HDMs), where new CP-violating effects can appear in the Yukawa couplings and in the Higgs potential. We focus on the 2HDM with softly broken Z_2 symmetry to avoid flavor-changing neutral current [65], which can contain a

Funded by SCOAP[3]

source of CP violation in the Higgs potential. Under the symmetry the possible Yukawa couplings are classified into four types (Types I, II, X, and Y) [66,67]. In the CP-conserving case these types of Yukawa interaction can predict different patterns of deviations in the Higgs boson couplings, by which we are able to fingerprint each model if any of the deviation is detected in the couplings by precision measurements [68–70]. Here we calculate the SM-like Higgs boson couplings to fermions and gauge bosons (*hff* and *hVV*) in these 2HDMs with the CP-violating phase. The current data for the scaling factors for Higgs boson couplings from the Large Hadron Collider (LHC) are the following values: $\kappa_Z = 1.07 \pm 0.10$, $\kappa_W = 1.07 \pm 0.11$, $\kappa_\tau = 1.02^{+0.17}_{-0.16}$, and $\kappa_b = 0.97^{+0.24}_{-0.22}$ at 1σ [71]. We show here how the effects of CP violation can be indirectly observed by precision measurements of the Higgs boson couplings at future collider experiments such as the International Linear Collider (ILC [72–74], FCC-ee [75], CEPC [76], and CLIC [77]).

2. 2HDM with softly broken Z_2 symmetry

Here we introduce the 2HDMs with softly broken discrete symmetry Z_2, which is introduced to avoid flavor-changing neutral current [65]. Isospin doublet scalar fields Φ_1 and Φ_2 are transformed under the Z_2 symmetry: $\Phi_1 \to \Phi_1$, $\Phi_2 \to -\Phi_2$. The Higgs potential is given by

$$\begin{aligned} V =& \mu_1^2(\Phi_1^\dagger\Phi_1) + \mu_2^2(\Phi_2^\dagger\Phi_2) - \{\mu_3^2(\Phi_1^\dagger\Phi_2) + \text{h.c.}\} + \frac{1}{2}\lambda_1(\Phi_1^\dagger\Phi_1)^2 + \frac{1}{2}\lambda_2(\Phi_2^\dagger\Phi_2)^2 \\ &+ \lambda_3(\Phi_1^\dagger\Phi_1)(\Phi_2^\dagger\Phi_2) + \lambda_4(\Phi_1^\dagger\Phi_2)(\Phi_2^\dagger\Phi_1) + \left\{\frac{1}{2}\lambda_5(\Phi_1^\dagger\Phi_2)^2 + \text{h.c.}\right\}, \end{aligned} \tag{1}$$

where μ_3^2 and λ_5 are generally complex, while the other parameters are real. Φ_1 and Φ_2 can be parametrized as

$$\Phi_1 = \begin{pmatrix} w_1^+ \\ \frac{1}{\sqrt{2}}(v_1 + h_1 + iz_1) \end{pmatrix}, \quad \Phi_2 = \begin{pmatrix} w_2^+ \\ \frac{1}{\sqrt{2}}(v_2 e^{i\xi} + h_2 + iz_2) \end{pmatrix}, \tag{2}$$

where $v^2 \equiv (v_1)^2 + (v_2)^2 = (\sqrt{2}G_\text{F})^{-1} = (246\ \text{GeV})^2$, G_F being the Fermi coupling constant. In this paper, we use the redefinition of phases of doublet fields to absorb the ξ. We then define the complex parameters μ_3^2 and λ_5 as $\text{Re}[\mu_3^2] + i\text{Im}[\mu_3^2]$ and $\text{Re}[\lambda_5] + i\text{Im}[\lambda_5]$, respectively.

The stationary conditions are given by

$$\left.\frac{\partial V}{\partial h_1}\right|_{\omega_j^+ = h_j = z_j = 0} = 0, \quad \left.\frac{\partial V}{\partial h_2}\right|_{\omega_j^+ = h_j = z_j = 0} = 0, \quad \left.\frac{\partial V}{\partial z_1}\right|_{\omega_j^+ = h_j = z_j = 0} = 0 \quad (j = 1, 2), \tag{3}$$

which lead to the following equations:

$$\mu_1^2 = \frac{M^2}{v^2}v_2^2 - \frac{1}{2}(\lambda_1 v_1^2 + \lambda_{345}v_2^2), \quad \mu_2^2 = \frac{M^2}{v^2}v_1^2 - \frac{1}{2}(\lambda_2 v_2^2 + \lambda_{345}v_1^2), \quad 2\text{Im}[\mu_3^2] = v_1 v_2 \text{Im}[\lambda_5], \tag{4}$$

where $\lambda_{345} \equiv \lambda_3 + \lambda_4 + \text{Re}[\lambda_5]$ and $M^2 \equiv v^2\text{Re}[\mu_3^2]/v_1 v_2$. There is one CP-violating parameter in the Higgs potential by using the third equation in Eq. (4). In this paper, we treat $\text{Im}[\lambda_5]$ as one physical parameter of CP violation.

We introduce the mixing angle β ($\tan\beta = v_2/v_1$) in order to rotate the original basis to the Higgs basis [78]:

$$\begin{pmatrix} \phi_1 \\ \phi_2 \end{pmatrix} = \begin{pmatrix} \cos\beta & \sin\beta \\ -\sin\beta & \cos\beta \end{pmatrix} \begin{pmatrix} \Phi_1 \\ \Phi_2 \end{pmatrix}, \quad \phi_1 = \begin{pmatrix} G^+ \\ \frac{1}{\sqrt{2}}(v + h_1' + iG^0) \end{pmatrix}, \quad \phi_2 = \begin{pmatrix} H^+ \\ \frac{1}{\sqrt{2}}(h_2' + ih_3') \end{pmatrix}, \tag{5}$$

where G^+, G^0 are Nambu–Goldstone boson states. In this basis, the mass of $H^\pm$ is

$$m_{H^\pm}^2 = M^2 - \frac{1}{2}v^2(\lambda_4 + \mathrm{Re}[\lambda_5]). \tag{6}$$

The mass matrix for h_1', h_2', and h_3' is not yet diagonalized, and takes the form [19,79]:

$$\mathcal{M}^2 = \begin{pmatrix} \tilde{m}_h^2 \sin^2(\beta-\tilde{\alpha}) + \tilde{m}_H^2 \cos^2(\beta-\tilde{\alpha}) & \frac{1}{2}(\tilde{m}_h^2 - \tilde{m}_H^2)\sin 2(\beta-\tilde{\alpha}) & -\frac{1}{2}v^2\mathrm{Im}[\lambda_5]\sin 2\beta \\ \frac{1}{2}(\tilde{m}_h^2 - \tilde{m}_H^2)\sin 2(\beta-\tilde{\alpha}) & \tilde{m}_h^2\cos^2(\beta-\tilde{\alpha}) + \tilde{m}_H^2\sin^2(\beta-\tilde{\alpha}) & -\frac{1}{2}v^2\mathrm{Im}[\lambda_5]\cos 2\beta \\ -\frac{1}{2}v^2\mathrm{Im}[\lambda_5]\sin 2\beta & -\frac{1}{2}v^2\mathrm{Im}[\lambda_5]\cos 2\beta & \tilde{m}_A^2 \end{pmatrix}, \tag{7}$$

where $\tilde{m}_h$, $\tilde{m}_H$, and $\tilde{m}_A$ are masses of the SM-like Higgs boson, extra CP-even, and CP-odd Higgs bosons in the CP-conserving limit, respectively. In this limit, $\tilde{\alpha}$ is the mixing angle that diagonalizes two CP-even states in the Higgs basis. We use an orthogonal matrix R in order to diagonalize the 3×3 mass matrix in Eq. (7):

$$R^T\mathcal{M}^2R = \mathrm{diag}(m_{H_1}^2, m_{H_2}^2, m_{H_3}^2). \tag{8}$$

We treat the mass eigenstate H_1 as the (discovered) SM-like Higgs boson with the mass 125 GeV. There are nine independent parameters in the potential in the following analysis:

$$v, M, m_{H^\pm}, m_{H_1}, \tilde{m}_H, \tilde{m}_A, \tilde{\alpha}, \tan\beta, \mathrm{Im}[\lambda_5]. \tag{9}$$

Next, we introduce Yukawa interactions and gauge interactions for H_1 in the model. Under the Z_2 symmetry, the Yukawa interaction is given by

$$-\mathcal{L}_{\mathrm{Yukawa}} = Y_u\bar{Q}_L(i\sigma_2\Phi_u^*)u_R + Y_d\bar{Q}_L\Phi_d d_R + Y_l\bar{L}_L\Phi_l l_R + \mathrm{h.c.}, \tag{10}$$

where $\Phi_{u,d,l}$ are either Φ_1 or Φ_2 by the charge assignment of the Z_2 symmetry for fields in the model. There are four types of Yukawa interactions [66,67], as shown in Table 1. Yukawa interactions for H_1 can then be rewritten as

$$-\mathcal{L}_{\mathrm{Yukawa}} \ni \sum_{f=u,d,l}\frac{m_f}{v}\bar{f}\left\{(R_{11} + R_{21}\xi_f) + (-2I_f)i\gamma_5R_{31}\xi_f\right\}fH_1, \tag{11}$$

where R_{ij} is the (i,j) component of the matrix R, ξ_f; they depend on the 2HDM type and are summarized in Table 2. I_f is the third component of the isospin for the fermion.

Gauge-coupling constants to H_1 take the following form:

$$\mathcal{L}_{\mathrm{kin}} \ni R_{11}\left\{\frac{2m_W^2}{v}W_\mu^+W^{-\mu} + \frac{m_Z^2}{v}Z_\mu Z^\mu\right\}H_1 = R_{11}\left\{g_{hWW}^{\mathrm{SM}}W_\mu^+W^{-\mu} + \frac{1}{2}g_{hZZ}^{\mathrm{SM}}Z_\mu Z^\mu\right\}H_1. \tag{12}$$

The scaling factors for H_1VV ($V = W$ and Z) are given at tree level by

$$\kappa_V \equiv \frac{g_{H_1VV}}{g_{hVV}^{\mathrm{SM}}} = R_{11}. \tag{13}$$

Table 1. Z_2 charge assignment for fermions and scalar bosons in each type [67].

	Φ_1	Φ_2	Q_L	L_L	u_R	d_R	l_R
Type I	+	−	+	+	−	−	−
Type II	+	−	+	+	−	+	+
Type X	+	−	+	+	−	−	+
Type Y	+	−	+	+	−	+	−

Table 2. ξ_f factor for each type [67].

	ξ_u	ξ_d	ξ_l
Type I	$+\cot\beta$	$+\cot\beta$	$+\cot\beta$
Type I	$+\cot\beta$	$-\tan\beta$	$-\tan\beta$
Type X	$+\cot\beta$	$+\cot\beta$	$-\tan\beta$
Type Y	$+\cot\beta$	$-\tan\beta$	$+\cot\beta$

There are theoretical bounds on the parameter space in the 2HDM with CP violation. The vacuum stability condition for the Higgs potential is given in Ref. [80]. The perturbative unitarity bounds on the two-body elastic scattering amplitudes for the gauge and Higgs bosons are given in Refs. [79,81].

The constraints from the S, T, and U parameters are seen in Refs. [82–84]. Parameters in the 2HDM are constrained by direct searches for additional Higgs bosons in the data from LHC Run-1 and Run-2 [85–89]. In addition, flavor experiments such as B meson decays give the lower limit on $m_{H^\pm}$ and $\tan\beta$ for each type [90,91]. New CP-violating effects in the new physics models are constrained by the EDM. The bounds from the EDM experiments on the parameter space of the 2HDM with CP violation have been discussed in Refs. [92,93].

3. Numerical analysis

In order to examine how CP-violating phases in the Higgs sector affect the Higgs boson couplings, we evaluate the scaling factors κ_V defined in Eq. (13) and the ratio of the decay rate for $H_1 \to f\bar{f}$, identifying H_1 as the discovered Higgs boson with a mass of 125 GeV and a decay rate for $h \to f\bar{f}$ in the SM:

$$\frac{\Gamma_{\rm 2HDM}(H_1 \to f\bar{f})}{\Gamma_{\rm SM}(h \to f\bar{f})} = (c_f^s)^2 + (c_f^p)^2 \left(1 - \frac{4m_f^2}{m_{H_1}^2}\right)^{-1}, \tag{14}$$

where

$$c_f^s = R_{11} + R_{21}\xi_f, \quad c_f^p = (-2I_f)R_{31}\xi_f. \tag{15}$$

The ratio of the decay rates coincides with that given in Ref. [94]. In the following numerical analysis, we take four of the nine parameters in Eq. (9) as

$$v = 246\,\text{GeV}, \quad m_{H_1} = 125\,\text{GeV}, \quad \tilde{m}_H = 200\,\text{GeV}, \quad \tilde{m}_A = 250\,\text{GeV}. \tag{16}$$

Here the relatively small masses for $\tilde{m}_H$ and $\tilde{m}_A$ are taken so that CP-violating effects are not greatly suppressed. Since the ratio of the decay rates is independent of M and $m_{H^\pm}$ at tree level, we can take values of M and $m_{H^\pm}$ to avoid the current constraints from the S, T, and U parameters [95]. We

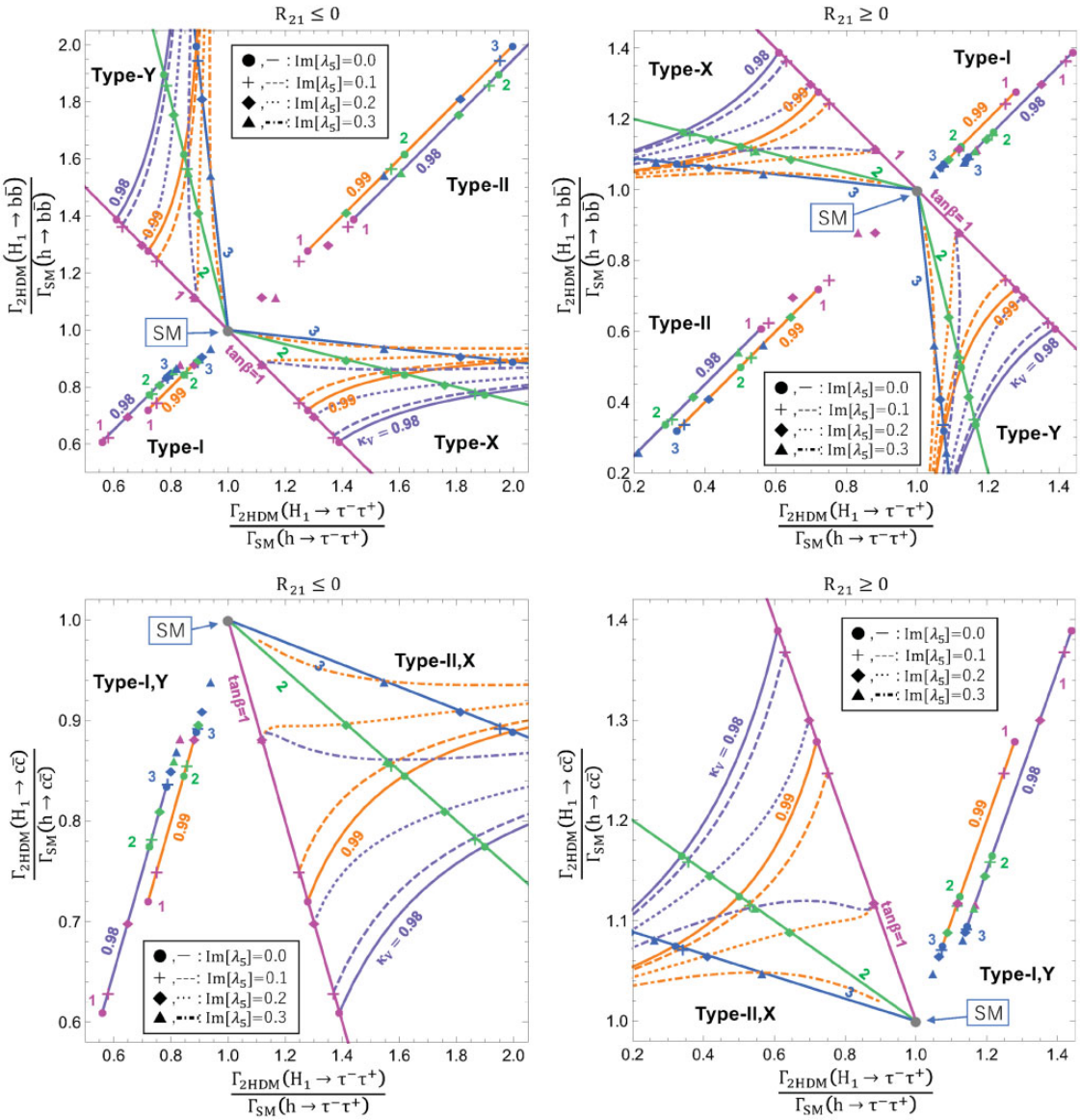

Fig. 1. The ratio of decay rate for $H_1 \to \tau^-\tau^+$, $H_1 \to b\bar{b}$ (top), and $H_1 \to c\bar{c}$ (bottom) with $R_{21} \leq 0$ (left) and $R_{21} \geq 0$ (right). The purple and orange lines correspond to $\kappa_V = 0.98$ and 0.99. The magenta, green, and blue lines and points correspond to $\tan\beta = 1$, 2, and 3. The dashed lines, dotted lines, and dot-dashed lines correspond to $\mathrm{Im}[\lambda_5] = 0.1$, 0.2, and 0.3, respectively. The cross, rhombus, and triangular points respectively move away from the circular points for the CP-conserving case by $\mathrm{Im}[\lambda_5] = 0.1, 0.2$, and 0.3. The (1.0, 1.0) point corresponds to the SM. We shift the purple lines of Types I and II in the upper panel and those of Types I and Y in the lower panel sideways, because the actual lines coincide with the orange lines.

show the numerical results for the scaling factor and the ratio of the decay rates, varying the rest of the parameters ($\tan\beta$, $\tilde{\alpha}$, and $\mathrm{Im}[\lambda_5]$). In the CP-conserving limit, $\cos(\beta - \tilde{\alpha})$ corresponds to R_{21}.

In Fig. 1, we show the ratio of decay rates for various final states of fermions in Types-I, II, X and Y 2HDM for several values of $\mathrm{Im}[\lambda_5]$ (= 0.0, 0.1, 0.2, and 0.3). In the upper panels, the results are shown on the plane of the decay into $\tau^-\tau^+$ and that into $b\bar{b}$, while in the lower panels, those on the plane of the decay into $\tau^-\tau^+$ and that into $c\bar{c}$ are shown. In the left-hand panels, the results for $R_{21} \leq 0$ are shown, while in the right-hand panels those for $R_{21} \geq 0$ are shown. In each panel, the (1.0, 1.0) point corresponds to the SM. Values of $\tan\beta$ are taken to be 1, 2, and 3, and those of

κ_V are 0.99 and 0.98. The purple lines for Types I and II in the upper panels and Types I and Y in the lower panels are moved slightly sideways from the original positions, which coincide with the orange lines. For each type of 2HDM, the purple (orange) solid, dashed, dotted, and dot-dashed lines correspond to the cases with $\mathrm{Im}[\lambda_5] = 0.0, 0.1, 0.2$, and 0.3 for $\kappa_V = 0.98$ ($\kappa_V = 0.99$), respectively. For Types X and Y in the upper panels and Types II and X in the lower panels, the magenta, green, and blue solid lines respectively correspond to $\tan\beta = 1$, 2, and 3. The cross, rhombus, and triangular points show how the predictions differ from the CP-conserving cases marked with circles, where the cross, rhombus, and triangular points correspond to $\mathrm{Im}[\lambda_5] = 0.1$, 0.2, and 0.3, respectively. We note that Fig. 1 contains the parameter regions excluded by the latest experimental results, in order to show the behavior of the ratios of the decay rates in each 2HDM type. The ratio of decay rates for various final states of fermions approaches $\kappa_V^2 + (1-\kappa_V^2)\xi_f^2$ when $\mathrm{Im}[\lambda_5]$ increases. For $\tan\beta = 1$ ($\tan\beta = 2$) with $\kappa_V = 0.99$, the mass of $m_{H_1} = 125$ GeV cannot be realized for $\mathrm{Im}[\lambda_5] > 0.22$ ($\mathrm{Im}[\lambda_5] > 0.28$). Therefore, the triangular points ($\mathrm{Im}[\lambda_5] = 0.3$) for those cases are not shown in the figure, and the orange dot-dashed lines are broken at the points (with $\tan\beta \simeq 2.2$) where m_{H_1} cannot be 125 GeV. For the parameters of Eq. (16), we may be able to distinguish not only the types of 2HDM [69] but also CP-violating cases from CP-conserving cases by the precision measurement of the Higgs boson couplings, as seen in Fig. 1. However, we cannot distinguish the ratios of decay rates with CP-violating effects from those in the CP-conserving 2HDM when $\tilde{m}_A$ is very large.

In Fig. 2, we show whether we can distinguish the CP-violating case from the CP-conserving case by using the ILC with $\sqrt{s} = 250$ GeV and $\mathcal{L} = 2$ ab^{-1}. We focus on the ratio of decay rates for $H_1 \to f\bar{f}$ ($f = \tau,\ b$, and c) and the scaling factor κ_V for H_1VV in Types I and X, because in Types II and Y the parameters in Eq. (16) are excluded by the constraints from the S, T, and U parameters and $b \to s\gamma$ [67]. In order to see how the CP-violating case can be distinguished from the CP-conserving case, we first do not take into account the EDM results in Fig. 2. Later, in Fig. 3, the results where the EDM constraints are taken into account are shown. In the upper panels, the results in Type I are shown on the plane of the ratio of decay rates for $H_1 \to f\bar{f}$ ($f = \tau,\ b$, and c) and the scaling factor κ_V for H_1VV, while in the lower panels, those in Type X on the plane of the decay into $\tau^-\tau^+$ and that into $b\bar{b}$ are shown. In the left-hand panels, the results for $R_{21} \le 0$ are shown, while in the right-hand panels those for $R_{21} \ge 0$ are shown. For Type-I 2HDM, the magenta (green and blue) solid, dashed, dotted, and dot-dashed lines correspond to the cases with $\mathrm{Im}[\lambda_5] = 0.0, 0.1, 0.2$, and 0.3 for $\tan\beta = 1$ ($\tan\beta = 2$ and 3), respectively. For Type X, the magenta, green, gray, and blue solid lines respectively correspond to $\tan\beta = 1, 2, 2.5$, and 3. The cross, rhombus, and triangular points in Fig. 2 are the same as those in Fig. 1. As fiducial points, we take the green triangular point ($\tan\beta = 2$ and $\mathrm{Im}[\lambda_5] = 0.3$) with $\kappa_V = 0.98$ in the upper panels, while we take the gray triangular point ($\tan\beta = 2.5$ and $\mathrm{Im}[\lambda_5] = 0.3$) with $\kappa_V = 0.99$ in the lower panels. Areas of 1σ accuracy from the fiducial point are shown as blue belts in the figures. These belts are shifted from the SM point in order to show whether we can distinguish the CP-violating 2HDM from the CP-conserving one by the precision measurement of the Higgs couplings in future experiments. Based on Ref. [72], we show the expected sensitivities for the future precision measurements of $H_1b\bar{b}$, $H_1c\bar{c}$, $H_1\tau^+\tau^-$, and H_1ZZ, which are taken to be 1.8%, 2.4%, 1.9%, and 0.38% at 1σ accuracy, respectively. The belts for H_1VV in the figure correspond to the sensitivity for H_1ZZ. The blue belts of the sensitivity for $H_1f\bar{f}$ in the upper panels correspond to the sensitivity for $H_1b\bar{b}$. In the lower panels the blue belts for κ_V are taken for the orange solid lines ($\kappa_V = 0.99$ and $\mathrm{Im}[\lambda_5] = 0$).

In the upper panels, the fiducial points and the blue circular points with $\kappa_V = 0.98$ are in the region where the blue belts of the sensitivity for $H_1f\bar{f}$ and H_1VV overlap. In this case, we cannot distinguish

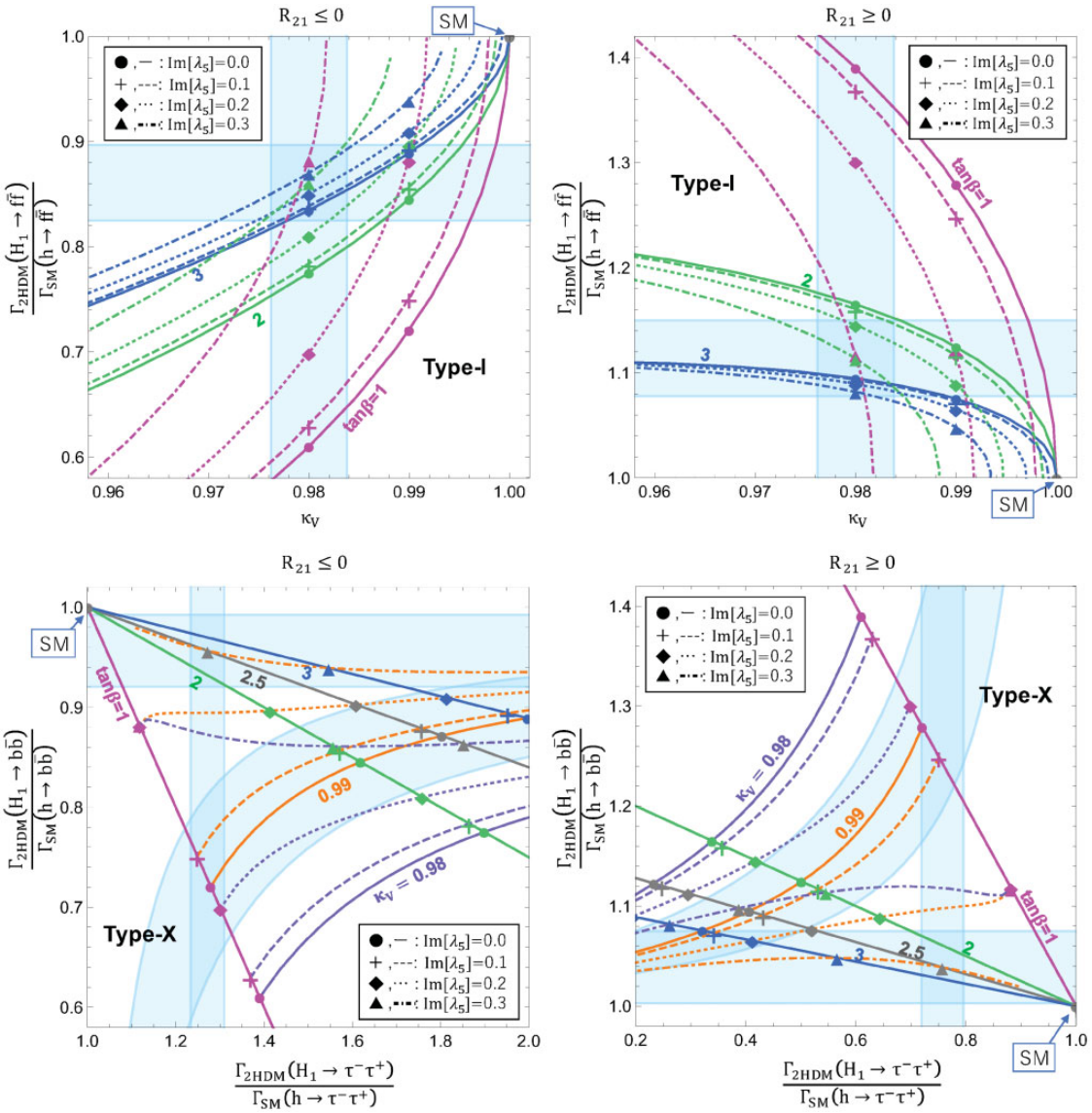

Fig. 2. The ratios of decay rate for the fermion and the scaling factors for the gauge boson in Type I (top) and Type X (bottom) with $R_{21} \leq 0$ (left) and $R_{21} \geq 0$ (right). The gray-colored lines in the lower panel are tan β=2.5. The other colored lines, all kinds of lines, and the marks are the same as those in Fig. 1. The blue belts indicate the sensitivity region of the ILC with 250 GeV and $\mathcal{L} = 2\,\text{ab}^{-1}$ at 1σ accuracy [72]. The blue belt for κ_V is the sensitivity region of H_1ZZ. In the upper panels, the blue belt for the vertical axis is the sensitivity region of $H_1b\bar{b}$. The center values of the sensitivity for H_1VV and $H_1f\bar{f}$ in the upper panels are at the green triangular point for $\kappa_V = 0.98$. In the lower panels, the sensitivity for H_1VV is along the orange solid line for $\kappa_V = 0.99$, while the center values of it for $H_1b\bar{b}$ and $H_1\tau^-\tau^+$ are at the gray triangular point for $\kappa_V = 0.99$.

the CP-violating case from the CP-conserving one in the Higgs sector by the precision measurements of Higgs boson couplings, unless tan β is determined accurately. In the CP-conserving case for Type X with $\kappa_V = 0.99$, the ratios of decay rates for the fermion should be on the orange solid line. However, the gray triangle for $\kappa_V = 0.99$ is away from the blue belt of the sensitivity for hVV in the lower panels. In the CP-conserving case, the ratios of decay rates for $H_1 \to \tau^-\tau^+$, $H_1 \to b\bar{b}$, and $H_1 \to c\bar{c}$ are completely determined by giving a set of κ_V and tan β at tree level. The gray triangle cannot be predicted in the CP-conserving case under the situation that $\kappa_V = 0.99$. This implies that

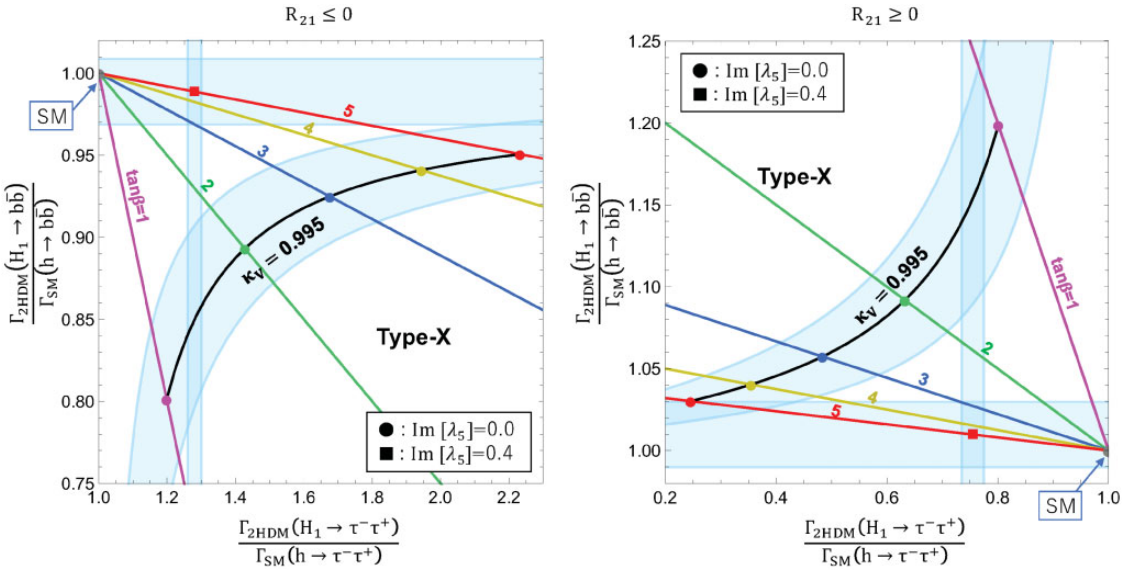

Fig. 3. The ratios of decay rate for the fermion and the scaling factors for the gauge boson in Type X with $R_{21} \leq 0$ (left) and $R_{21} \geq 0$ (right). The magenta, green, blue, yellow, and red solid lines and points in the figure respectively correspond to $\tan\beta = 1,\ 2,\ 3,\ 4$, and 5. All points correspond to $\kappa_V = 0.995$. The red square point, which is not excluded by the EDM analysis based on Ref. [92], corresponds to $\mathrm{Im}[\lambda_5] = 0.4$. The blue belts correspond to the sensitivity region for $H_1 b\bar{b}$, $H_1\tau^-\tau^+$, and $H_1 VV$, which are about 1%, 1%, and 0.2% precision respectively at 1σ accuracy. The sensitivity for $H_1 VV$ is along the black solid line for $\kappa_V = 0.995$ and $\mathrm{Im}[\lambda_5]$=0, while that for $H_1 b\bar{b}$ and $H_1\tau^-\tau^+$ is on the red square point for $\kappa_V = 0.995$.

we may be able to distinguish the CP-violating case from the CP-conserving case by the precision measurements of Higgs boson couplings κ_V and decay rates $\Gamma(H_1 \to \tau^-\tau^+)$, $\Gamma(H_1 \to b\bar{b})$, and $\Gamma(H_1 \to c\bar{c})$ at the ILC with $\sqrt{s} = 250$ GeV and $\mathcal{L} = 2$ ab^{-1}. We note that the fiducial points in the figure are already excluded by the EDM.

In the Type-I 2HDM taking into account the EDM data, we confirmed that we cannot distinguish the CP-violating case from the CP-conserving case via precision measurements of Higgs boson couplings, because the ratios of decay rate for the fermion and the scaling factors for the gauge boson in these cases overlap. Therefore, in Fig. 3, we only show the results in the Type-X 2HDM under the constraint from the EDM data. In the left-hand panels, the results for $R_{21} \leq 0$ are shown, while in the right-hand panels those for $R_{21} \geq 0$ are shown. The magenta, green, blue, yellow, and red solid lines in the figure respectively correspond to $\tan\beta = 1, 2, 3, 4$, and 5. In the Type-X 2HDM, $|c_u^p| < 3 \times 10^{-2}$, with c_u^p given in Eq. (15), is allowed by the EDM data [92]. There is another constraint on $\mathrm{Im}[\lambda_5]$ with respect to satisfying the mass 125 GeV of the Higgs boson. In the Type-X 2HDM, if $\mathrm{Im}[\lambda_5] > 0.41$, we cannot explain the Higgs mass of 125 GeV. Therefore, in the figure the red square point ($\mathrm{Im}[\lambda_5] = 0.4$) is taken as a fiducial point and the point is allowed by the EDM data. In addition, this fiducial point is allowed by the theoretical bounds [79–81] and other experimental data such as electroweak precision tests ($S = 0.05 \pm 0.10$, $T = 0.08 \pm 0.12$, and $U = 0.02 \pm 0.10$ [95]), the current data for the scaling factors for Higgs boson couplings ($\kappa_Z = 1.07 \pm 0.10$, $\kappa_\tau = 1.02^{+0.17}_{-0.16}$, and $\kappa_b = 0.97^{+0.24}_{-0.22}$ at 1σ [71]), the direct search of H^+ by the data from LHC Run-2 (the lower limit on $m_{H^\pm}$ being about 150 GeV at 95% confidence level in the Type-X 2HDM with $\tan\beta \simeq 5$ by $H^+ \to \tau\nu$ [89]), and B meson decay (the lower limit on $m_{H^\pm}$ being about 80 GeV at 95% confidence level in the Type-X 2HDM with $\tan\beta \geq 2$ by $B_s^0 \to \mu^+\mu^-$ [90]). The location of the red square point for the CP-violating case is away from that of the red circular

Table 3. The CP mixing angles $\psi_{\rm CP}$ for the red square point in Fig. 3.

		$\mathrm{Im}[\lambda_5]$	$\psi_{\rm CP}$
Type X	$(R_{21} \leq 0)$	0.4	-26°
Type X	$(R_{21} \geq 0)$	0.4	-30°

point for the CP-conserving case with the same values of $\tan\beta$ and κ_V. The blue belts in the figure correspond to the expected sensitivities for the future precision measurements of the Higgs boson couplings $H_1 b\bar{b}$, $H_1\tau^-\tau^+$, and $H_1 VV$, which are taken to be 1%, 1%, and 0.2% at 1σ accuracy. Such accuracy could be achieved at the ILC with $\sqrt{s} = 250$ GeV if the integrated luminosity is enhanced to be $\mathcal{L} = 8$ ab^{-1}. In the figure, the blue belts for $H_1 b\bar{b}$ and $H_1\tau^-\tau^+$ are on the red square point ($\mathrm{Im}[\lambda_5] = 0.4$), and the belt for the scaling factor κ_V is along the black line for the CP-conserving case with $\kappa_V = 0.995$.

Consequently, in the Type-I 2HDM it is difficult to distinguish the CP-violating case from the CP-conserving case by very precise measurements of the Higgs boson couplings. On the other hand, in the Type-X 2HDM we may be able to detect the CP-violating effect by very precise measurement of the Higgs boson couplings even in the case favored by the EDM data, if the integrated luminosity is large enough. We note that in the Type-X 2HDM with $R_{21} \geq 0$ we cannot distinguish the red square points for the CP-violating case with $\mathrm{Im}[\lambda_5] = 0.4$ from the points with $\tan\beta = 18$–19, $\kappa_V = 0.995$, and $\mathrm{Im}[\lambda_5] = 0$. However, in the CP-conserving 2HDM, the case with such large $\tan\beta$ values with $\kappa_V = 0.995$ is already excluded by current data [71,96].

Here we give a comment that the angular distribution of $H_1 \to \tau^-\tau^+$ can be used to measure the CP-violating effect in the Higgs sector [13]. The CP mixing angle $\psi_{\rm CP}$ is given by

$$\mathcal{L}_{H_1\tau\tau} = g\bar{\tau}(\cos\psi_{\rm CP} + i\gamma_5 \sin\psi_{\rm CP})\tau H_1, \tag{17}$$

where $g = -m_\tau\sqrt{(c_\tau^s)^2 + (c_\tau^p)^2}/v$ with c_τ^s and c_τ^p given in Eq. (15). At the ILC with $\sqrt{s} = 250$ GeV and $\mathcal{L} = 2$ ab^{-1}, $\psi_{\rm CP}$ can be measured to a precision of 4.3° [13]. In the Type-I 2HDM where the EDM data are taken into account, we cannot detect the CP-violating effect by measuring the angular distribution of $H_1 \to \tau^-\tau^+$ at the ILC. On the other hand, in the Type-X 2HDM the corresponding values of $\psi_{\rm CP}$ to the red square points in Fig. 3 are given in Table 3. We can complementarily examine the effects of CP violation in the Type-X 2HDM by precision measurements of the Higgs boson couplings and the angular distribution of $H_1 \to \tau^-\tau^+$ at future Higgs factories.

4. Summary

We have studied how the effects of CP violation can be observed indirectly by precision measurements of the coupling constants of the Higgs boson with the mass 125 GeV at a future Higgs factory such as the ILC. We have investigated the difference between CP-conserving and CP-violating cases of 2HDMs with softly broken discrete symmetry. We have found that in some parameter sets the CP-violating effects in the extended Higgs sectors can be detected by measuring the Higgs boson couplings very precisely.

Note added: A paper on a new electron EDM bound was published after we finished our work [97]. The fiducial points in Fig. 3 may be excluded by these experimental data. Since the Higgs boson couplings deviate from one in the CP-conserving case due to the parameters of CP violation, such

as Im[λ_5], which is allowed by the new EDM data, we may be able to distinguish the CP-violating 2HDM from the CP-conserving one by very precise measurements of Higgs boson couplings.

Acknowledgements

The work of M.A. is supported in part by the Japan Society for the Promotion of Sciences (JSPS) Grant-in-Aid for Scientific Research (Grant No. 25400250 and No. 16H00864). K.H. and M.K. are supported by the Sasakawa Scientific Research Grant from The Japan Science Society. The work of S.K. is supported in part by a Grant-in-Aid for Scientific Research on Innovative Areas, the Ministry of Education, Culture, Sports, Science and Technology, No. 16H06492 and No. 18H04587, Grant H2020-MSCA-RISE-2014 No. 645722 (Non-Minimal Higgs), and the JSPS Joint Research Projects (Collaboration, Open Partnership) "New frontier of neutrino mass generation mechanisms via Higgs physics at LHC and flavor physics".

Funding

Open Access funding: SCOAP[3].

References

[1] G. Aad et al. [ATLAS Collaboration], Phys. Lett. B **716**, 1 (2012).
[2] S. Chatrchyan et al. [CMS Collaboration], Phys. Lett. B **716**, 30 (2012).
[3] V. A. Kuzmin, V. A. Rubakov, and M. E. Shaposhnikov, Phys. Lett. B **155**, 36 (1985).
[4] J. R. Dell'Aquila and C. A. Nelson, Nucl. Phys. B **320**, 61 (1989).
[5] G. R. Bower, T. Pierzchała, Z. Wąs, and M. Worek, Phys. Lett. B **543**, 227 (2002).
[6] K. Desch, Z. Was, and M. Worek, Eur. Phys. J. C **29**, 491 (2003).
[7] R. Harnik, A. Martin, T. Okui, R. Primulando, and F. Yu, Phys. Rev. D **88**, 076009 (2013).
[8] S. Berge, W. Bernreuther, and J. Ziethe, Phys. Rev. Lett. **100**, 171605 (2008).
[9] S. Berge and W. Bernreuther, Phys. Lett. B **671**, 470 (2009).
[10] S. Berge, W. Bernreuther, B. Niepelt, and H. Spiesberger, Phys. Rev. D **84**, 116003 (2011).
[11] S. Berge, W. Bernreuther, and H. Spiesberger, Phys. Lett. B **727**, 488 (2013).
[12] K. Hagiwara, K. Ma, and S. Mori, Phys. Rev. Lett. **118**, 171802 (2017).
[13] D. Jeans and G. W. Wilson, Phys. Rev. D **98**, 013007 (2018).
[14] A. Méndez and A. Pomarol, Phys. Lett. B **272**, 313 (1991).
[15] W. Bernreuther and A. Brandenburg, Phys. Rev. D **49**, 4481 (1994).
[16] W. Khater and P. Osland, Nucl. Phys. B **661**, 209 (2003).
[17] E. Asakawa, S. Y. Choi, K. Hagiwara, and J. S. Lee, Phys. Rev. D **62**, 115005 (2000).
[18] E. Asakawa and K. Hagiwara, Eur. Phys. J. C **31**, 351 (2003).
[19] V. Keus, S. F. King, S. Moretti, and K. Yagyu, J. High Energy Phys. **1604**, 048 (2016).
[20] B. Grzadkowski, O. M. Ogreid, and P. Osland, J. High Energy Phys. **1605**, 025 (2016); **1711**, 002 (2017) [erratum].
[21] O. M. Ogreid, P. Osland, and M. N. Rebelo, J. High Energy Phys. **1708**, 005 (2017).
[22] L. Bian, N. Chen, and Y. Zhang, Phys. Rev. D **96**, 095008 (2017).
[23] C. Y. Chen, H. L. Li, and M. Ramsey-Musolf, Phys. Rev. D **97**, 015020 (2018).
[24] H. Bélusca-Maïto, A. Falkowski, D. Fontes, J. C. Romão, and J. P. Silva, J. High Energy Phys. **1804**, 002 (2018).
[25] P. Basler, M. Mühlleitner, and J. Wittbrodt, J. High Energy Phys. **1803**, 061 (2018).
[26] D. Fontes, M. Mühlleitner, J. C. Romão, R. Santos, J. P. Silva, and J. Wittbrodt, J. High Energy Phys. **1802**, 073 (2018).
[27] D. Azevedo, P. Ferreira, M. Margarete Mühlleitner, R. Santos, and J. Wittbrodt, Phys. Rev. D **99**, 055013 (2019) [arXiv:1808.00755 [hep-ph]] [Search INSPIRE].
[28] S. Kanemura, Y. Okada, and E. Senaha, Phys. Lett. B **606**, 361 (2005).
[29] A. Noble and M. Perelstein, Phys. Rev. D **78**, 063518 (2008).
[30] M. Aoki, S. Kanemura, and O. Seto, Phys. Rev. Lett. **102**, 051805 (2009).
[31] M. Aoki, S. Kanemura, and O. Seto, Phys. Rev. D **80**, 033007 (2009).
[32] M. Aoki, S. Kanemura, and K. Yagyu, Phys. Rev. D **83**, 075016 (2011).
[33] S. Kanemura, E. Senaha, and T. Shindou, Phys. Lett. B **706**, 40 (2011).

[34] C. Tamarit, Phys. Rev. D **90**, 055024 (2014).
[35] S. Kanemura, N. Machida, and T. Shindou, Phys. Lett. B **738**, 178 (2014).
[36] K. Hashino, S. Kanemura, and Y. Orikasa, Phys. Lett. B **752**, 217 (2016).
[37] M. Kakizaki, S. Kanemura, and T. Matsui, Phys. Rev. D **92**, 115007 (2015).
[38] K. Hashino, M. Kakizaki, S. Kanemura, and T. Matsui, Phys. Rev. D **94**, 015005 (2016).
[39] M. Kamionkowski, A. Kosowsky, and M. S. Turner, Phys. Rev. D **49**, 2837 (1994).
[40] J. Kehayias and S. Profumo, J. Cosmol. Astropart. Phys. **1003**, 003 (2010).
[41] A. D. Dolgov, D. Grasso, and A. Nicolis, Phys. Rev. D **66**, 103505 (2002).
[42] C. Grojean and G. Servant, Phys. Rev. D **75**, 043507 (2007).
[43] J. R. Espinosa, T. Konstandin, J. M. No, and M. Quiros, Phys. Rev. D **78**, 123528 (2008).
[44] C. Caprini et al., J. Cosmol. Astropart. Phys. **1604**, 001 (2016).
[45] S. J. Huber, T. Konstandin, G. Nardini, and I. Rues, J. Cosmol. Astropart. Phys. **1603**, 036 (2016).
[46] P. S. B. Dev and A. Mazumdar, Phys. Rev. D **93**, 104001 (2016).
[47] M. Chala, G. Nardini, and I. Sobolev, Phys. Rev. D **94**, 055006 (2016).
[48] P. Huang, A. J. Long, and L. T. Wang, Phys. Rev. D **94**, 075008 (2016).
[49] A. Kobakhidze, A. Manning, and J. Yue, Int. J. Mod. Phys. D **26**, 1750114 (2017).
[50] A. Addazi, Mod. Phys. Lett. A **32**, 1750049 (2017).
[51] K. Hashino, M. Kakizaki, S. Kanemura, P. Ko, and T. Matsui, Phys. Lett. B **766**, 49 (2017).
[52] Z. Kang, P. Ko, and T. Matsui, J. High Energy Phys. **1802**, 115 (2018).
[53] W. Chao, W. F. Cui, H. K. Guo, and J. Shu, arXiv:1707.09759 [hep-ph] [Search INSPIRE].
[54] S. V. Demidov, D. S. Gorbunov, and D. V. Kirpichnikov, Phys. Lett. B **779**, 191 (2018).
[55] Y. Chen, M. Huang, and Q. S. Yan, J. High Energy Phys. **1805**, 178 (2018).
[56] M. Chala, C. Krause, and G. Nardini, J. High Energy Phys. **1807**, 062 (2018).
[57] K. Hashino, M. Kakizaki, S. Kanemura, P. Ko, and T. Matsui, J. High Energy Phys. **1806**, 088 (2018).
[58] T. Vieu, A. P. Morais, and R. Pasechnik, arXiv:1802.10109 [hep-ph] [Search INSPIRE].
[59] S. Bruggisser, B. von Harling, O. Matsedonskyi, and G. Servant, Phys. Rev. Lett. **121**, 131801 (2018) [arXiv:1803.08546 [hep-ph]] [Search INSPIRE].
[60] B. Imtiaz, Y. Wan, and Y.-F. Cai, Eur. Phys. J. C **79**, 25 (2019) [arXiv:1804.05835 [hep-ph]] [Search INSPIRE].
[61] F. P. Huang, Z. Qian, and M. Zhang, Phys. Rev. D **98**, 015014 (2018).
[62] S. Bruggisser, B. von Harling, O. Matsedonskyi, and G. Servant, J. High Energy Phys. **1812**, 099 (2018) [arXiv:1804.07314 [hep-ph]] [Search INSPIRE].
[63] M. F. Axen, S. Banagiri, A. Matas, C. Caprini, and V. Mandic, Phys. Rev. D **98**, 103508 (2018) [arXiv:1806.02500 [astro-ph.IM]] [Search INSPIRE].
[64] E. Megías, G. Nardini, and M. Quirós, J. High Energy Phys. **1809**, 095 (2018) [arXiv:1806.04877 [hep-ph]] [Search INSPIRE].
[65] S. L. Glashow and S. Weinberg, Phys. Rev. D **15**, 1958 (1977).
[66] V. Barger, J. L. Hewett, and R. J. N. Phillips, Phys. Rev. D **41**, 3421 (1990).
[67] M. Aoki, S. Kanemura, K. Tsumura, and K. Yagyu, Phys. Rev. D **80**, 015017 (2009).
[68] S. Kanemura, M. Kikuchi, and K. Yagyu, Phys. Lett. B **731**, 27 (2014).
[69] S. Kanemura, K. Tsumura, K. Yagyu, and H. Yokoya, Phys. Rev. D **90**, 075001 (2014).
[70] S. Kanemura, M. Kikuchi, K. Mawatari, K. Sakurai, and K. Yagyu, Phys. Lett. B **783**, 140 (2018).
[71] The ATLAS collaboration [ATLAS Collaboration], ATLAS-CONF-2018-031 (available at: https://atlas.web.cern.ch/Atlas/GROUPS/PHYSICS/CONFNOTES/ATLAS-CONF-2018-031/).
[72] K. Fujii et al., arXiv:1710.07621 [hep-ex] [Search INSPIRE].
[73] H. Baer et al., arXiv:1306.6352 [hep-ph] [Search INSPIRE].
[74] S. Asai et al., arXiv:1710.08639 [hep-ex] [Search INSPIRE].
[75] M. Bicer et al. [TLEP Design Study Working Group], J. High Energy Phys. **1401**, 164 (2014).
[76] M. Ahmad et al. [CEPC-SPPC Study Group], IHEP-CEPC-DR-2015-01, IHEP-TH-2015-01, IHEP-EP-2015-01 (available at: http://cepc.ihep.ac.cn/preCDR/volume.html).
[77] M. J. Boland et al. [CLIC and CLICdp Collaborations], arXiv:1608.07537 [physics.acc-ph] [Search INSPIRE].
[78] S. Davidson and H. E. Haber, Phys. Rev. D **72**, 035004 (2005); **72**, 099902 (2005) [erratum].
[79] S. Kanemura and K. Yagyu, Phys. Lett. B **751**, 289 (2015).
[80] B. Grzadkowski, O. M. Ogreid, and P. Osland, Phys. Rev. D **80**, 055013 (2009).
[81] I. F. Ginzburg and I. P. Ivanov, Phys. Rev. D **72**, 115010 (2005).

[82] M. E. Peskin and T. Takeuchi, Phys. Rev. Lett. **65**, 964 (1990).
[83] M. E. Peskin and T. Takeuchi, Phys. Rev. D **46**, 381 (1992).
[84] H. E. Haber and D. O'Neil, Phys. Rev. D **83**, 055017 (2011).
[85] J. Bernon, J. F. Gunion, H. E. Haber, Y. Jiang, and S. Kraml, Phys. Rev. D **92**, 075004 (2015).
[86] S. Chang, S. K. Kang, J. P. Lee, and J. Song, Phys. Rev. D **92**, 075023 (2015).
[87] G. C. Dorsch, S. J. Huber, K. Mimasu, and J. M. No, Phys. Rev. D **93**, 115033 (2016).
[88] L. Wang, F. Zhang, and X.-F. Han, Phys. Rev. D **95**, 115014 (2017).
[89] A. Arbey, F. Mahmoudi, O. Stål, and T. Stefaniak, Eur. Phys. J. C **78**, 182 (2018).
[90] T. Enomoto and R. Watanabe, J. High Energy Phys. **1605**, 002 (2016).
[91] M. Misiak and M. Steinhauser, Eur. Phys. J. C **77**, 201 (2017).
[92] K. Cheung, J. S. Lee, E. Senaha, and P.-Y. Tseng, J. High Energy Phys. **1406**, 149 (2014).
[93] T. Abe, J. Hisano, T. Kitahara, and K. Tobioka, J. High Energy Phys. **1401**, 106 (2014); **1604**, 161 (2016) [erratum].
[94] J. Shu and Y. Zhang, Phys. Rev. Lett. **111**, 091801 (2013).
[95] C. Patrignani et al. [Particle Data Group], Chin. Phys. C **40**, 100001 (2016) and 2017 update (available at: http://pdg.lbl.gov/2017/reviews/contents_sports.html).
[96] CMS Collaboration, CMS-PAS-HIG-17-011.
[97] V. Andreev et al. [ACME Collaboration], Nature **562**, 355 (2018).